

Microscopic Observation of Heavy Quasiparticle Formation in the Intermediate Valence Compound EuNi_2P_2 : ^{31}P NMR Study

Nonoka Higa¹, Mamoru Yogi^{2*}, Hiroko Kuroshima¹, Tatsuki Toji¹, Haruo Niki², Yuichi Hiranaka¹, Ai Nakamura¹, Takao Nakama², Masato Hedo², and Yoshichika Ōnuki²

¹Graduate School of Engineering and Science, University of the Ryukyus, Nishihara, Okinawa 903-0213, Japan

²Faculty of Science, University of the Ryukyus, Nishihara, Okinawa 903-0213, Japan

We report ^{31}P NMR measurements under various magnetic fields up to 7 T for the intermediate valence compound EuNi_2P_2 , which shows heavy electronic states at low temperatures. In the high-temperature region above 40 K, the Knight shift followed the Curie–Weiss law reflecting localized $4f$ states. In addition, the behavior corresponding to the temperature variation of the average valence of Eu was observed in the nuclear spin-lattice relaxation rate $1/T_1$. With the occurrence of the Kondo effect, $1/T_1$ was clearly reduced below 40 K, and the Knight shift becomes almost constant at low temperatures. From these results, the formation of heavy quasiparticles by the hybridization of Eu $4f$ electrons and conduction electrons was clarified from microscopic viewpoints. Furthermore, a characteristic spin fluctuation was observed at low temperatures, which would be associated with valence fluctuations caused by the intermediate valence state of EuNi_2P_2 .

1. Introduction

The localization and itinerancy of the f electron in rare-earth compounds are closely related to their ground states. The Kondo effect and the Ruderman–Kittel–Kasuya–Yosida (RKKY) interaction are important interactions between f electrons and conduction electrons, and the elucidation of specific physical properties in the vicinity of the quantum critical point (QCP), where these interactions are competing, is one of the essential themes in the strongly correlated electron system.^{1,2)} After the discovery of the well-known first heavy electron superconductor CeCu_2Si_2 ,³⁾ many studies have been conducted on peculiar physical properties near the antiferromagnetic QCP.^{1,2)} Superconductivity was also found in the ferromagnetic materials UGe_2 , URhGe , and UCoGe .^{4–7)} The electronic states near the ferromagnetic QCP with pressure application and the magnetic field have also attracted considerable attention, and many research studies have been carried out.

The relationship between the valence states of f electrons and novel electronic states is also being studied. For example, it has been reported that the superconducting transition temperature T_c of CeCu_2Si_2 is greatly enhanced by applying pressure.^{8,9)} The crossover of the valence of Ce is experimentally observed at around 4 GPa where T_c is maximum,¹⁰⁾ and the occurrence of superconductivity due to valence fluctuations is theoretically discussed.¹¹⁾ In addition, a heavy electronic state in Yb compounds has been found in $\text{YbCo}_2\text{Zn}_{20}$ and $\beta\text{-YbAlB}_4$.^{12,13)} It has been reported that $\beta\text{-YbAlB}_4$ shows not only a heavy electronic state but also quantum criticality different from that of the Doniach diagram, which is often observed in Ce compounds.¹⁴⁾ The valence of Yb in $\beta\text{-YbAlB}_4$ is estimated to be +2.75, and the intermediate va-

lence (mixed-valence) state is presumably related to the novel ground state of $\beta\text{-YbAlB}_4$.¹⁵⁾ Thus, the valence instability of rare-earth ions plays an important role in the emergence of novel physical properties.

In this study, we focus on the rare-earth element Eu, which has two kinds of valence states Eu^{2+} ($4f^7$) and Eu^{3+} ($4f^6$). The divalent Eu state is magnetic ($J = S = 7/2$, $L = 0$), where J is the total angular momentum, S is the spin angular momentum, and L is the orbital angular momentum. Therefore, intermetallic compounds with divalent Eu ions tend to order magnetically at low temperatures, following the RKKY interaction.^{16,17)} The pressure effect on divalent Eu compounds is often different from that of Ce compounds. For example, in EuNi_2Ge_2 and EuRh_2Si_2 , a valence transition from a divalent state to an almost trivalent state occurs above the critical pressure P_V , and a nonmagnetic ground state is realized.^{18–21)} On the other hand, some compounds, such as EuPt_2Si_2 , behave following the Doniach diagram. The antiferromagnetic transition temperature T_N of EuPt_2Si_2 decreases continuously with increasing pressure without showing the valence transition, and $T_N = 0$ at $P_V \approx 4$ GPa.^{22,23)} Unlike the divalent Eu state, the trivalent Eu state is nonmagnetic ($J = 0$, $S = L = 3$). EuPd_3 is one of the few Eu compounds in which the Eu ion becomes trivalent.^{24–26)} The specific heat and magnetic susceptibility of EuPd_3 are analyzed using the J -multiplet levels 7F_J with $J = 0 - 6$.^{27,28)}

Among Eu compounds, EuNi_2P_2 takes an intermediate valence state and shows a significant temperature variation in the average valence. It has been reported from Mössbauer measurements that the average valence of Eu is +2.25 at 300 K, and it increases with decreasing temperature and becomes +2.50 at 1.4 K.²⁹⁾ Specific heat measurements down to 80 mK have revealed that EuNi_2P_2 shows no magnetic order and

*myogi@sci.u-ryukyu.ac.jp

forms a heavy electronic state with a large electronic specific heat coefficient $\gamma = 93 \text{ mJ}/(\text{K}^2\cdot\text{mol})$ at low temperatures.^{30,31} For the trivalent compound EuPd_3 , the electronic specific heat coefficient was obtained as $\gamma = 3.6 \text{ mJ}/(\text{K}^2\cdot\text{mol})$.²⁸ Therefore, the intermediate valence state of Eu plays an important role in the formation of the heavy electronic state in EuNi_2P_2 . The hybridization between the Eu $4f$ electrons and conduction electrons was reported from studies of photoemission spectroscopy, X-ray magnetic circular dichroism, and optical conductivity.^{32–35} In these circumstances, we carried out ^{31}P NMR measurements on EuNi_2P_2 to clarify its electronic state from a microscopic viewpoint. We report on the static magnetic properties and low-energy fluctuations of EuNi_2P_2 from the measurements of resonance spectra and relaxation rates under various magnetic fields up to 7 T.

2. Experimental Procedure

Single crystals of EuNi_2P_2 were grown by the Sn-flux method. Details of the sample preparation are described elsewhere.^{31,36} The crystals were powdered to facilitate applied rf-field penetration. The NMR measurement was performed on ^{31}P nucleus (nuclear spin $I = 1/2$) by a conventional spin-echo method using a conventional phase-coherent pulsed spectrometer in the temperature range of $T = 1.6\text{--}300 \text{ K}$. The NMR spectra were obtained by sweeping the frequency and integrating the spin-echo signal intensity step by step. The Knight shift was referred to the ^{31}P resonance frequency of phosphoric acid solution, $\nu_0 \equiv (^{31}\gamma_n/2\pi)\mu_0H$. Here, $^{31}\gamma_n$ is the nuclear gyromagnetic ratio of ^{31}P and μ_0H is an external magnetic field. The nuclear spin-lattice relaxation time T_1 was measured by a saturation-recovery method.

3. Results and Analysis

3.1 NMR spectrum and Knight shift

Figure 1 shows the ^{31}P NMR spectra of EuNi_2P_2 measured in an external magnetic field $\mu_0H = 1.0 \text{ T}$ at temperatures $T = 300$ and 4.2 K . At 300 K , a sharp spectrum with a line width of 190 kHz was observed. With decreasing temperature, the line width increases, and the peak position shifts to the low-frequency side. Since ^{31}P has no nuclear quadrupole moment, the resonance frequency ν_m can be described as

$$\nu_m = \nu_0 [1 + K(\theta)]. \quad (1)$$

Here, $K(\theta)$ is the Knight shift, and θ is the angle between the external magnetic field and the c -axis of the crystal. From the local symmetry of the P site in EuNi_2P_2 ($4mm$ in Hermann-Mauguin notation or international notation), the Knight shift has axisymmetric anisotropy. In this case, the Knight shift can be written as $K(\theta) = K_{\text{iso}} + K_{\text{an}}(3 \cos^2 \theta - 1)$ using the isotropic shift K_{iso} and the anisotropic shift K_{an} . The characteristic powder patterns should be observed when we use randomly oriented powder samples. The shape of the obtained spectrum indicates no remarkable anisotropy in the Knight shift. The spectrum at 4.2 K shows a tail to the low-frequency side, which possibly corresponds to anisotropy appearing in magnetic susceptibility below about 50 K .³¹

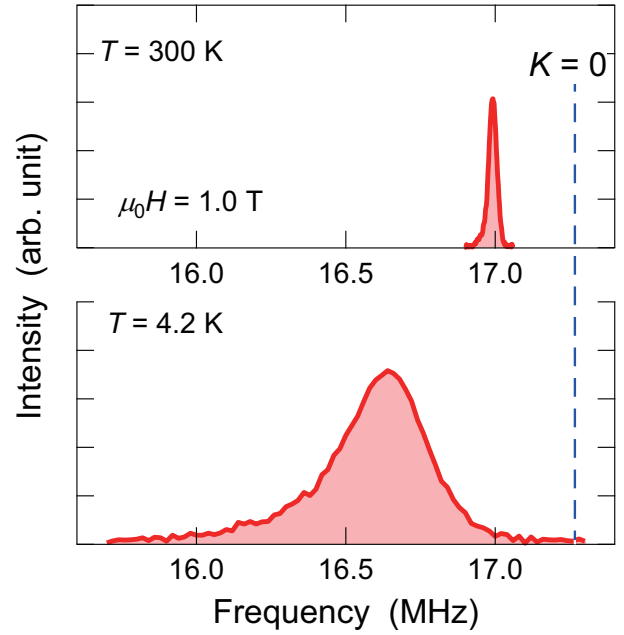


Fig. 1. (Color online) ^{31}P NMR spectra of EuNi_2P_2 in $\mu_0H = 1.0 \text{ T}$ at $T = 300$ and 4.2 K .

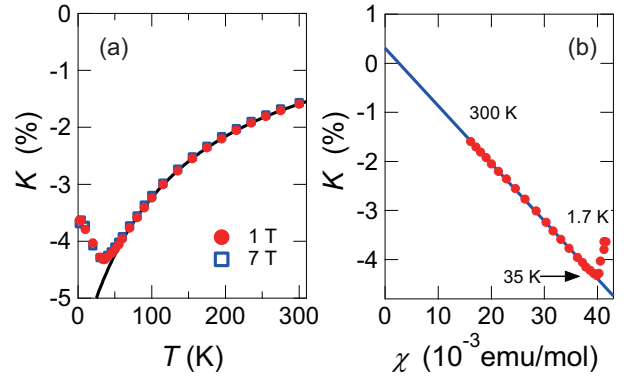


Fig. 2. (Color online) (a) Temperature dependences of the Knight shift at $\mu_0H = 1.0$ and 7.0 T . The solid curve indicates a Curie–Weiss fit. (b) K vs χ plot with T as implicit parameter. The solid line indicates $K = [A_{\text{hf}} / (N_A \mu_B)] \chi$ with hyperfine coupling constant $A_{\text{hf}} = -6.53 \text{ kOe}/\mu_B$.

Since the anisotropy of the spectrum was small as described above, the Knight shift was determined by the peak position of the spectrum. The temperature dependences of the Knight shift measured under the magnetic fields $\mu_0H = 1.0$ and 7.0 T are shown in Fig. 2(a). The obtained Knight shift at $\mu_0H = 1.0 \text{ T}$ is in agreement with the previously reported results^{37,38} and shows no significant magnetic field dependence up to $\mu_0H = 7.0 \text{ T}$. This indicates that the static magnetic and valence states of Eu are not affected by the magnetic field. In addition, the Knight shift has a negative value in the whole measurement temperature range, indicating that the core polarization due to $2p$ electrons is a major contribution to the Knight shift. In

general, the Knight shift consists of the sum of the spin part K_s and the orbital part K_{orb} . Here, assuming K_s obeys the Curie–Weiss law and K_{orb} is independent of temperature, the Knight shift can be written as

$$K(T) = \frac{C}{T - \theta} + K_{\text{orb}}. \quad (2)$$

The solid line in Fig. 2(a) is the result of the fitting for the experimental data above 100 K with C , θ and K_{orb} being the free parameters. We obtained $C = -768$ %K, $\theta = -121.8$ K, and $K_{\text{orb}} = 0.23\%$. The fitted line is in good agreement with the experimental data, which means that the static magnetic properties are dominated by the localized moments of the $4f$ electrons in Eu at the high-temperature region. A divalent state of Eu has no total orbital angular momentum ($L = 0$). Therefore, the finite K_{orb} is presumed to be due to the intermediate valence state of Eu in EuNi_2P_2 .

At low temperatures below about 70 K, the Knight shift deviates from the Curie–Weiss behavior and shows a minimum at 40 K. At the lowest temperature, the Knight shift becomes almost constant. These characteristic behaviors indicate the formation of a heavy electron state due to the Kondo effect. Figure 2(b) shows the K vs χ plot. There is a good linearity above 35 K; however, a change in the slope is observed at lower temperatures. Such behavior was observed in many heavy-fermion compounds,³⁹⁾ the origin of which is due to the change in the hyperfine coupling constant associated with heavy quasiparticle formation. Thus, the $K - \chi$ plot suggests the formation of a heavy electron state at low temperatures. The relationship between the hyperfine coupling constant of A_{hf} of ^{31}P and the magnetic susceptibility χ can be expressed as

$$K = \frac{A_{\text{hf}}}{N_A \mu_B} \chi, \quad (3)$$

where N_A is Avogadro's number and μ_B is the Bohr magneton. The hyperfine coupling constant of $A_{\text{hf}} = -6.53$ kOe/ μ_B is estimated from the slope of the solid line, which is fitted to the experimental data above 30 K.

3.2 Analysis of T_1

To investigate the electronic state furthermore, the nuclear magnetization recovery curve was measured at the peak frequency of the ^{31}P NMR spectrum. When an electronic state is homogeneous, the recovery curve for $I = 1/2$ is generally described as a single exponential function given by

$$1 - \frac{M_z(t)}{M_0} = e^{-\frac{t}{T_1}}, \quad (4)$$

where M_0 and $M_z(t)$ are the nuclear magnetization at the thermal equilibrium condition and the nuclear magnetization at a time t after the saturation pulse, respectively. Figures 3(a)–3(c) show the recovery curve measured at temperatures of 1.7, 20, and 100 K, with $\mu_0 H = 7.0$ T. Above 100 K, we can fit the data well by Eq. (4) as indicated by the solid line in Fig. 3(a) and determine T_1 uniquely. However, the recovery curve begins to deviate from the single exponential behavior below

about 80 K. This suggests that the electronic state becomes inhomogeneous below about 80 K for some reason. In this case, the two-component fit is often employed. The two-component fit means that two electronic states corresponding to each T_1 are mixed; however, it is unlikely to occur in EuNi_2P_2 . Instead, the analysis assuming the distribution of T_1 is more plausible. The stretch exponential function $\exp\left[-\left(\frac{t}{T_1}\right)^\beta\right]$ is often used for the analysis of the recovery curve when T_1 is distributed. Detailed studies of the value and distribution of T_1 of the stretch exponential function for the exponent β were reported.^{40,41)} Since the distribution of T_1 changes with the exponent β , it is necessary to pay attention to the analysis using the stretch exponential recovery function when β shows a temperature variation. On the other hand, an analysis assuming the Gaussian distribution of $1/T_1$ on a logarithmic scale has been reported by Mitrović et al.⁴²⁾ According to that, the recovery curve can be written as follows

$$M_G(t) = \int \mathcal{P}_{\sigma_{\log}, W_1}(R_1) e^{-tR_1} d(\log_{10} R_1). \quad (5)$$

Here, $\mathcal{P}_{\sigma_{\log}, W_1}(R_1)$ describes the relaxation rate distribution given by

$$\mathcal{P}_{\sigma_{\log}, W_1}(R_1) = \frac{1}{\sigma_{\log}} \sqrt{\frac{2}{\pi}} e^{-\frac{2(\log_{10} R_1 - \log_{10} W_1)^2}{\sigma_{\log}^2}}, \quad (6)$$

where σ_{\log} is the width of the distribution on a \log_{10} scale and W_1 is the center of the Gaussian. Therefore, W_1 is considered as the most plausible relaxation rate. As an example, the distributions of the relaxation rate calculated with $W_1 = 1$ and various σ_{\log} are shown in Fig. 3(d). In the limit of $\sigma_{\log} \rightarrow 0$, Eq. (5) becomes single exponential, resulting in Eq. (4). Therefore, we regard W_1 as $1/T_1$ in the following discussion. The dashed lines in Figs. 3(b) and 3(c) are fit using Eq. (5), which reproduces the experimental data well. We analyzed the recovery curve at each temperature using Eq. (5), and obtained T_1 and its distribution σ_{\log} . The distribution of $1/T_1$ below 80 K increases with decreasing temperature as seen in Fig. 3(e).

The temperature dependence of $1/T_1$ at $\mu_0 H = 7.0$ T obtained by the analysis mentioned above is shown in Fig. 3(f). The distribution of $1/T_1$ is also displayed as a color plot. $1/T_1$ shows an almost constant behavior at around 300 K and begins to decrease slightly below about 200 K. A further distinct decrease in $1/T_1$ is observed below 40 K. At the lowest temperature, $1/T_1$ is almost proportional to temperature, indicating that the Fermi-liquid state with heavy quasiparticles is realized.

For further investigation, the magnetic field dependence of $1/T_1$ was measured. In all the measured magnetic fields, the recovery curves below 80 K deviate from the single exponential behavior. The temperature dependence of $1/T_1$ obtained using Eq. (5) in various magnetic fields is shown in Fig. 4. In the high-temperature region above 15 K, $1/T_1$ is not affected by the magnetic field. On the other hand, a significant magnetic field dependence was observed below 15 K, revealing

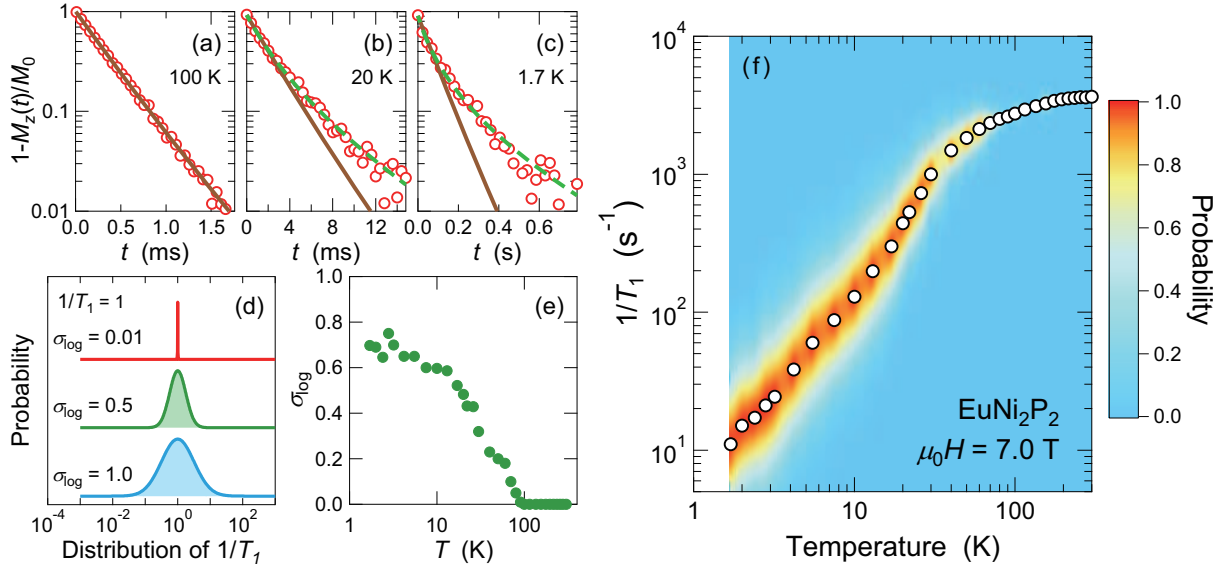


Fig. 3. (color online) (a), (b), and (c) ^{31}P nuclear magnetization recovery curves at $T = 100$, 20, and 1.7 K, respectively. The solid lines are a fit assuming a single T_1 . The dashed lines are a fit assuming the Gaussian distribution of T_1 on a logarithmic scale. (d) Gaussian probability distribution of $1/T_1$ in the case of various σ_{\log} . (e) T dependence of σ_{\log} at $\mu_0 H = 7.0$ T, showing a distribution of $1/T_1$ below ~ 80 K. (f) T dependence of $1/T_1$ at $\mu_0 H = 7.0$ T. A distribution of $1/T_1$ is displayed by a color plot.

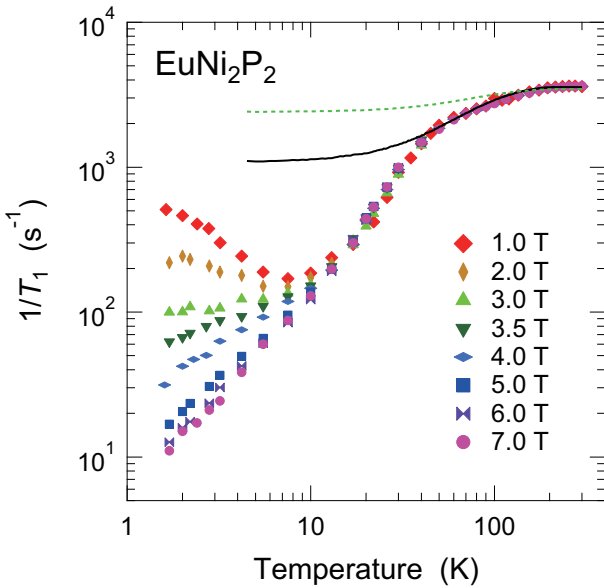


Fig. 4. (Color online) T dependence of $1/T_1$ under various external magnetic fields. The dotted and solid lines indicate calculation results assuming that $1/T_1$ is related to the average valence of Eu.

the development of the spin fluctuations in low-temperature and low-magnetic-field regions.

4. Discussion

We discuss the relationship between the $4f$ electron state and $1/T_1$. As described above, $1/T_1$ is almost constant at around 300 K. When the nuclear magnetic relaxation is

caused by fluctuating local moment, $1/T_1$ is given by⁴³⁾

$$\frac{1}{T_1} = \sqrt{2\pi} (g\gamma_n A_{\text{hf}})^2 \frac{J(J+1)}{3\omega_{\text{fl}}}, \quad (7)$$

where ω_{fl} is the local moment fluctuation frequency, assumed as $\omega_{\text{fl}} \gg \gamma_n H$. If a fluctuation due to the exchange interaction between localized moments is dominant, ω_{fl} is given as ω_{ex} as

$$\omega_{\text{ex}} = \frac{k_B \theta_{\text{CW}}}{\hbar} \sqrt{\frac{6}{zJ(J+1)}}. \quad (8)$$

Here, z ($= 8$) is the number of nearest-neighbor moments. From the values of $\theta_{\text{CW}} = -121.8$ K and $A_{\text{hf}} = -6.53$ kOe/ μ_B obtained from the results of magnetic susceptibility and the Knight shift, the relaxation rate by the local moment fluctuation was estimated as $1/T_1 \sim 8 \times 10^4$ s $^{-1}$ for $J = 7/2$ of Eu^{2+} . The calculated $1/T_1$ is one order of magnitude larger than the experimental value, suggesting that there is another fluctuation that is different from the fluctuation derived from the exchange interaction. In the case of EuNi_2P_2 , the valence of Eu is reported to be $\text{Eu}^{2.25+}$ at 300 K.²⁹⁾ Therefore, the valence fluctuations between Eu^{2+} and Eu^{3+} affect the local moment fluctuation, and ω_{fl} may be expressed as $\omega_{\text{fl}} = \omega_{\text{ex}} + \omega_{\text{vf}}$. Here, ω_{vf} is a frequency of the valence fluctuation. The measured $1/T_1$ being smaller than the calculated value that takes ω_{ex} into consideration indicates the presence of valence fluctuations in EuNi_2P_2 .

According to Eq. (7), $1/T_1$ is constant regardless of temperature; however, the measured $1/T_1$ depends on temperature even in the high-temperature region as shown in Fig. 4. As described above, the $K - \chi$ plot shows a linear behavior, i.e., the hyperfine coupling constant does not change above

40 K. Therefore, the decrease in $1/T_1$ below 200 K reflects the change in the $4f$ electron state of Eu. It is reported from a Mössbauer experiment that the average valence of Eu in EuNi_2P_2 is changed to the nonmagnetic side with decreasing temperature.²⁹⁾ Hence, the temperature variation in $1/T_1$ near 200 K is presumably related to the average valence of Eu. Assuming that the nuclear magnetic relaxation by the local moment fluctuation of the $4f$ electron is derived from the Eu^{2+} state, $1/T_1^{\text{fl}}$ can be written as

$$\frac{1}{T_1^{\text{fl}}} = a(b - V_{\text{av}}). \quad (9)$$

Here, V_{av} is the average valence of Eu, and a and b are fitting parameters. If $1/T_1^{\text{fl}} = 0$ for the trivalent Eu state, $b = 3$. The dotted line in Fig. 4 is the calculated result with $b = 3$, which does not reproduce the measured $1/T_1$ well. In contrast, $1/T_1$ is well reproduced by $b = 2.58$ in a wide temperature range as shown by the solid line in Fig. 4. This indicates that the intermediate valence state is not a simple combination of divalent and trivalent states, and that the valence fluctuation plays an important role in low-energy spin fluctuations.

A remarkable decrease in $1/T_1$, compared with the estimated one from the temperature variation in the Eu average valence, was observed below $T^* \simeq 40$ K. This indicates that the shielding of the local moment due to conduction electrons, that is, the Kondo effect, is caused. The characteristic temperature T^* is close to the Kondo temperature $T_K \sim 80$ K determined from the electrical resistivity.³¹⁾ The temperature at which $1/T_1$ begins to distribute is close to T_K as shown in Figs. 3(e) and 3(f); therefore, the distribution of $1/T_1$ is considered to be associated with the distribution of T_K , which is presumed to be due to a slight inhomogeneity of the average valence. Since $1/T_1$ does not show a remarkable magnetic field dependence above 15 K, it is apparent that the valence state and Kondo effect are not affected by the magnetic field of about 7 T.

Next, we focus on the temperature range below 10 K. A clear magnetic field dependence was observed as shown in Fig. 4. An increase in $1/T_1$ accompanied by the development of spin fluctuation was observed at $\mu_0 H = 1.0$ T. An increase in the magnetic field suppresses the enhancement of $1/T_1$, and the $T_1 T = \text{const.}$ behavior inherent to the Fermi-liquid state is realized at $\mu_0 H = 7.0$ T. Fisher et al. also observed an anomaly at low temperatures from the specific heat measurements.³⁰⁾ The specific heat divided by temperature, C/T , shows an upturn below 5 K and is suppressed by the application of a magnetic field of 7 T. This behavior is similar to the magnetic field dependence of $1/T_1$. However, it has been pointed out that the anomaly in the low-temperature specific heat should be related to a small impurity contained in the sample,³⁰⁾ thus suggesting that the observed spin fluctuation in $1/T_1$ is also caused by impurities. Generally, the nuclear magnetic relaxation by impurities is easily suppressed by a small magnetic field. In EuNi_2P_2 , the magnetic field of about 7 T, as seen in Fig. 4, is required to suppress the spin fluctua-

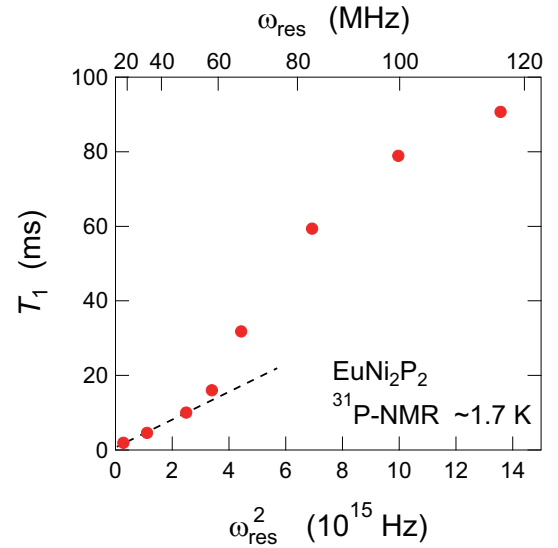


Fig. 5. (Color online) ω_{res}^2 dependence of T_1 at the lowest temperature. As indicated by the dashed line, a deviation from the linear relation occurs at more than about 50 MHz ($\mu_0 H \sim 3$ T).

tion at low temperatures. Therefore, it is unclear whether the anomaly observed in $1/T_1$ is caused by magnetic impurities or it is a novel phenomenon unique to the heavy electron state of the Eu compound with the intermediate valence state.

In addition, the influence of the nuclear magnetism of the Eu nucleus is also conceivable. For example, in $\text{PrFe}_4\text{P}_{12}$, relaxation by the nuclear magnetism of ^{141}Pr nuclei with a nuclear magnetic moment of $4.14\mu_N$ has been observed.⁴⁴⁾ The $1/T_1$ of $\text{PrFe}_4\text{P}_{12}$ in the low-temperature and low-magnetic-field regions showed a decrease with increasing magnetic field (resonant frequency ω_{res}). For the magnetic field dependence of $1/T_1$, the fluctuation of the ^{141}Pr nuclear magnetic moment was analyzed, and it was found that T_1 and ω_{res} follow the relation $T_1 = A + B\omega_{\text{res}}^2$. Here, A and B are parameters related to the characteristic frequency and magnitude of the fluctuation of the nuclear magnetic moment. From this result, it was concluded that the magnetic field dependence of $1/T_1$ of $\text{PrFe}_4\text{P}_{12}$ is due to the magnetism of ^{141}Pr nuclei. The linear relation between T_1 and ω_{res}^2 was also found in ^{17}O NMR in NpO_2 , which was explained by the cross-relaxation process by ^{237}Np nuclear spin.⁴⁵⁾ Eu has two isotopes, ^{151}Eu and ^{153}Eu , and their nuclear magnetic moments are $3.47\mu_N$ and $1.53\mu_N$, respectively. Therefore, the relaxation of the ^{31}P nucleus due to the fluctuation of the Eu nuclear dipole magnetic field may have been observed. To verify these, we plotted the ω_{res}^2 variation of T_1 at the lowest temperature as shown in Fig. 5. As is apparent from the dashed line in Fig. 5, a linear relation was seen only in a very narrow range of $\omega_{\text{res}} < 50$ MHz ($\mu_0 H \sim 3$ T). Although we cannot eliminate the possibility of Eu nuclear magnetism, we believe that the increase in $1/T_1$ is caused by characteristic fluctuations of other origins. To elucidate these points, further studies including those of other

heavy-fermion Eu compounds are required. Theoretical studies of the intermediate valence state and $c - f$ hybridization in Eu compounds are also expected.

5. Summary

To clarify the electronic state of the intermediate valence compound EuNi_2P_2 from the microscopic viewpoint, ^{31}P NMR measurements were carried out in various magnetic fields up to 7 T. In the high-temperature region, the Knight shift follows the Curie–Weiss law, indicating that the $4f$ electrons of Eu are localized. The localized $4f$ electronic state was also observed in $1/T_1$, and the temperature variation in $1/T_1$ corresponding to the change in the average valence of Eu was found. Below about 40 K, $1/T_1$ showed an apparent decrease with decreasing temperature. In addition, the absolute value of the Knight shift showed the maximum at approximately 40 K, and it became almost constant at low temperatures. These results reveal the occurrence of the Kondo effect in EuNi_2P_2 . $1/T_1$ exhibits a clear magnetic field dependence at low temperatures, which is attributed to the valence fluctuation caused by the intermediate valence state of EuNi_2P_2 .

Acknowledgments

We would like to thank K. Magishi, Y. Tokunaga, and K. Ishida for useful comments and discussion. This work was supported by JSPS KAKENHI Grant Numbers JP20102002, JP23540418, JP16K05453, JP17K05547 and JGC-S SCHOLARSHIP FOUNDATION.

- 1) H. v. Löhneysen, A. Rosch, M. Vojta, and P. Wölfle, *Rev. Mod. Phys.* **79**, 1015 (2007).
- 2) P. Gegenwart, Q. Si, and F. Steglich, *Nat. Phys.* **4**, 186 (2008).
- 3) F. Steglich, J. Aarts, C. D. Bredl, W. Lieke, D. Meschede, W. Franz, and H. Schäfer, *Phys. Rev. Lett.* **43**, 1892 (1979).
- 4) S. S. Saxena, P. Agarwal, K. Ahilan, F. M. Grosche, R. K. W. Haselwimmer, M. J. Steiner, E. Pugh, I. R. Walker, S. R. Julian, P. Monthoux, G. G. Lonzarich, A. Huxley, I. Sheikin, D. Braithwaite, and J. Flouquet, *Nature* **406**, 587 (2000).
- 5) D. Aoki, A. Huxley, E. Ressouche, D. Braithwaite, J. Flouquet, J.-P. Brison, E. Lhotel, and C. Paulsen, *Nature* **413**, 613 (2001).
- 6) F. Lévy, I. Sheikin, B. Grenier, and A. D. Huxley, *Science* **309**, 1343 (2005).
- 7) N. T. Huy, A. Gasparini, D. E. de Nijs, Y. Huang, J. C. P. Klaasse, T. Gortenmulder, A. de Visser, A. Hamann, T. Görlach, and H. v. Löhneysen, *Phys. Rev. Lett.* **99**, 067006 (2007).
- 8) H. Q. Yuan, F. M. Grosche, M. Deppe, C. Geibel, G. Sparn, and F. Steglich, *Science* **302**, 2104 (2003).
- 9) A. T. Holmes, D. Jaccard, and K. Miyake, *Phys. Rev. B* **69**, 024508 (2004).
- 10) T. C. Kobayashi, K. Fujiwara, K. Takeda, H. Harima, Y. Ikeda, T. Adachi, Y. Ohishi, C. Geibel, and F. Steglich, *J. Phys. Soc. Jpn.* **82**, 114701 (2013).
- 11) K. Miyake and S. Watanabe, *J. Phys. Soc. Jpn.* **83**, 061006 (2014).
- 12) M. S. Torikachvili, S. Jia, E. D. Mun, S. T. Hannahs, R. C. Black, W. K. Neils, D. Martien, S. L. Bud'ko, and P. C. Canfield, *PNAS* **104**, 9960 (2007).
- 13) S. Nakatsuji, K. Kuga, Y. Machida, T. Tayama, T. Sakakibara, Y. Karaki, H. Ishimoto, S. Yonezawa, Y. Maeno, E. Pearson, G. G. Lonzarich, L. Balicas, H. Lee, and Z. Fisk, *Nat. Phys.* **4**, 603 (2008).
- 14) T. Tomita, K. Kuga, Y. Uwatoko, P. Coleman, and S. Nakatsuji, *Science* **349**, 506 (2015).
- 15) M. Okawa, M. Matsunami, K. Ishizaka, R. Eguchi, M. Taguchi, A. Chainani, Y. Takata, M. Yabashi, K. Tamasaku, Y. Nishino, T. Ishikawa, K. Kuga, N. Horie, S. Nakatsuji, and S. Shin, *Phys. Rev. Lett.* **104**, 247201 (2010).
- 16) I. Felner, *J. Phys. Chem. Solids* **36**, 1063 (1975).
- 17) I. Felner and I. Nowik, *J. Phys. Chem. Solids* **39**, 767 (1978).
- 18) H. Wada, M. F. Hundley, R. Movshovich, and J. D. Thompson, *Phys. Rev. B* **59**, 1141 (1999).
- 19) A. Nakamura, T. Nakama, K. Uchima, N. Arakaki, C. Zukeran, S. Komesu, M. Takeda, Y. Takaesu, D. Nakamura, M. Hedo, K. Yagasaki, and Y. Uwatoko, *J. Phys.: Conf. Ser.* **400**, 032106 (2012).
- 20) A. Mitsuda, S. Hamano, N. Araoka, H. Yayama, and H. Wada, *J. Phys. Soc. Jpn.* **81**, 023709 (2012).
- 21) F. Honda, K. Okauchi, A. Nakamura, D. Li, D. Aoki, H. Akamine, Y. Ashitomi, M. Hedo, T. Nakama, and Y. Ōnuki, *J. Phys. Soc. Jpn.* **85**, 063701 (2016).
- 22) A. Mitsuda, T. Goto, N. Takeshita, N. Mori, H. Wada, and M. Shiga, *Acta Phys. Pol. B* **34**, 1149 (2003).
- 23) T. Takeuchi, T. Yara, Y. Ashitomi, W. Iha, M. Kakihana, M. Nakashima, Y. Amako, F. Honda, Y. Homma, D. Aoki, Y. Uwatoko, T. Kida, T. Tahara, M. Hagiwara, Y. Haga, M. Hedo, T. Nakama, and Y. Ōnuki, *J. Phys. Soc. Jpn.* **87**, 074709 (2018).
- 24) I. R. Harris and G. V. Raynor, *J. Less-Common Met.* **9**, 263 (1965).
- 25) I. R. Harris and G. Longworth, *J. Less-Common Met.* **23**, 281 (1971).
- 26) E.-J. Cho, S.-J. Oh, S. Suga, T. Suzuki, and T. Kasuya, *J. Electron Spectrosc. Relat. Phenom.* **77**, 173 (1996).
- 27) W. E. Gardner, J. Penfold, T. F. Smith, and I. R. Harris, *J. Phys. F: Met. Phys.* **2**, 133 (1972).
- 28) T. Takeuchi, A. Nakamura, M. Hedo, T. Nakama, and Y. Ōnuki, *J. Phys. Soc. Jpn.* **83**, 114001 (2014).
- 29) R. Nagarajan, G. K. Shenoy, L. C. Gupta, and E. V. Sampathkumaran, *Phys. Rev. B* **32**, 2846 (1985).
- 30) R. A. Fisher, P. Radhakrishna, N. E. Phillips, J. V. Badding, and A. M. Stacy, *Phys. Rev. B* **52**, 13519 (1995).
- 31) Y. Hirakawa, A. Nakamura, M. Hedo, T. Takeuchi, A. Mori, Y. Hirose, K. Mitamura, K. Sugiyama, M. Hagiwara, T. Nakama, and Y. Ōnuki, *J. Phys. Soc. Jpn.* **82**, 083708 (2013).
- 32) S. Danzenbächer, D. V. Vyalikh, Y. Kucherenko, A. Kade, C. Laubschat, N. Caroca-Canales, C. Krellner, C. Geibel, A. V. Fedorov, D. S. Dessau, R. Follath, W. Eberhardt, and S. L. Molodtsov, *Phys. Rev. Lett.* **102**, 026403 (2009).
- 33) Y. H. Matsuda, Z. W. Ouyang, H. Nojiri, T. Inami, K. Ohwada, M. Suzuki, N. Kawamura, A. Mitsuda, and H. Wada, *Phys. Rev. Lett.* **103**, 046402 (2009).
- 34) V. Guritanu, S. Seiro, J. Sichelschmidt, N. Caroca-Canales, T. Iizuka, S. Kimura, C. Geibel, and F. Steglich, *Phys. Rev. Lett.* **109**, 247207 (2012).
- 35) H. Anzai, K. Ichiki, E. F. Schwier, H. Iwasawa, K. Shimada, H. Namatame, M. Taniguchi, A. Mitsuda, H. Wada, and K. Mimura, *J. Phys.: Conf. Ser.* **807**, 012006 (2017).
- 36) R. Marchand and W. Jeitschko, *J. Solid State Chem.* **24**, 351 (1978).
- 37) E. V. Sampathkumaran, I. Stang, R. Vijayaraghavan, G. Kaindl, and K. Lüders, *Phys. Rev. B* **31**, 6099 (1985).
- 38) K. Magishi, R. Watanabe, A. Hisada, T. Saito, K. Koyama, and T. Fujiwara, *J. Phys.: Conf. Ser.* **592**, 012031 (2015).
- 39) N. J. Curro, B.-L. Young, J. Schmalian, and D. Pines, *Phys. Rev. B* **70**, 235117 (2004).
- 40) M. N. Berberan-Santos, E. N. Bodunov, and B. Valeur, *Chem. Phys.* **315**, 171 (2005).
- 41) D. C. Johnston, *Phys. Rev. B* **74**, 184430 (2006).
- 42) V. F. Mitrović, M.-H. Julien, C. de Vaulx, M. Horvatić, C. Berthier, T. Suzuki, and K. Yamada, *Phys. Rev. B* **78**, 014504 (2008).
- 43) T. Moriya, *Prog. Theor. Phys.* **16**, 641 (1956).
- 44) K. Ishida, H. Murakawa, K. Kitagawa, Y. Ihara, H. Kotegawa, M. Yogi, Y. Kitaoka, B.-L. Young, M. S. Rose, D. E. MacLaughlin, H. Sugawara, T. D. Matsuda, Y. Aoki, H. Sato, and H. Harima, *Phys. Rev. B* **71**, 024424

(2005).

45) Y. Tokunaga, R. E. Walstedt, Y. Homma, D. Aoki, S. Kambe, H. Sakai,

T. Fujimoto, S. Ikeda, E. Yamamoto, A. Nakamura, Y. Shiokawa, and
H. Yasuoka, Phys. Rev. B **74**, 064421 (2006).